Journal of Fluorine Chemistry 132 (2011) 732–739

Contents lists available at ScienceDirect

Journal of Fluorine Chemistry

journal homepage: www.elsevier.com/locate/fluor

$[H_3tren]^{3+}$ and $[H_4tren]^{4+}$ fluoride zirconates or tantalates

Mohamed Ali Saada [a], Vincent Maisonneuve [a], Jérome Marrot [b], Nicolas Mercier [c], Marc Leblanc [a], Annie Hémon-Ribaud [a,*]

[a] Laboratoire des Oxydes et Fluorures, UMR CNRS 6010, Faculté des Sciences et Techniques, Université du Maine, Avenue O. Messiaen, 72085 Le Mans Cedex 9, France
[b] Institut Lavoisier, UMR CNRS 8180, Université de Versailles Saint Quentin-en-Yvelines, 45 Avenue des Etats Unis, 75035 Versailles Cedex, France
[c] Laboratoire de Chimie Inorganique, Matériaux et Interfaces, UMR CNRS 6200, Université d'Angers, 2 Boulevard Lavoisier, 49045 Angers, France

ARTICLE INFO

Article history:
Received 1 April 2011
Received in revised form 6 May 2011
Accepted 10 May 2011
Available online 17 May 2011

Keywords:
Hybrid fluorides
Hydrothermal synthesis
Microwave heating

This article is dedicated to Dr. Alain Tressaud who is awarded the 2011 ACS price for his Creative Work in Fluorine Chemistry

ABSTRACT

Four new $[H_3tren]^{3+}$ or $[H_4tren]^{4+}$ fluoride zirconates and two new $[H_3tren]^{3+}$ fluoride tantalates are evidenced in the (ZrF_4 or Ta_2O_5)-*tren*-$HF_{aq.}$-ethanol systems at 190 °C: the structurally related phases $[H_4tren]\cdot(Zr_2F_{12})\cdot H_2O$ and α-$[H_4tren]\cdot(Zr_2F_{12})$ ($P2_12_12_1$), β-$[H_4tren]\cdot(Zr_2F_{12})$ ($P2_1/c$), $[H_3tren]_4\cdot(ZrF_8)_3\cdot 4H_2O$ ($I23$), β-$[H_3tren]_2\cdot(Ta_3O_2F_{16})\cdot(F)$ ($R32$) and its monoclinic distortion α-$[H_3tren]_2\cdot(Ta_3O_2F_{16})\cdot(F)$ ($C2/m$). α and β-$[H_4tren]\cdot(Zr_2F_{12})$ and $[H_4tren]\cdot(Zr_2F_{12})\cdot H_2O$ are built up from (Zr_2F_{12}) dimers of edge sharing ZrF_7 polyhedra while isolated ZrF_8 dodecahedra are found in $[H_3tren]_4\cdot(ZrF_8)_3\cdot 4H_2O$. Linear $(Ta_3O_2F_{16})$ trimers build α and β-$[H_3tren]_2\cdot(Ta_3O_2F_{16})\cdot(F)$; they consist of two $(TaOF_6)$ pentagonal bipyramids that are linked to two opposite oxygen atoms of one central (TaO_2F_4) octahedron. A disorder affects the equatorial fluorine atoms of the trimers and eventually carbon or nitrogen atoms of $[H_3tren]^{3+}$ cations.

1. Introduction

The quest to discover new porous materials is still intense. Unusual or recently discovered properties are very exciting: loading and release of antitumural and antiretroviral drugs [1] or CO_2 storage [2] with MIL-101. Most of this frenetic activity is aimed at developing oxide and oxyanion-based open structures with giant pores. Success is due in part to the introduction of fluoride ion from HF solutions in order to promote the crystallization of hybrid organic–inorganic solids. Several research groups tend to insert F^- as a unique metal ligand. A recent review is devoted to the structural aspects of such hybrid metal fluorides [3] in which phases with three dimensionally (3D) interconnected pores are scarce. Only four hybrid phases with open structures are reported: $[Hmeam]\cdot(Li_2Be_2F_7)$ [4], $[H_2en]_{0.5}\cdot(Y_2F_7)$ [5], $[H_2dap]_{0.5}\cdot(Y_3F_{10})$ [6] and $(H_3O)\cdot[Hgua]_5\cdot(ZrF_5)_6$ [7]. Most often, hybrid metal fluorides are prepared by hydrothermal or solvothermal synthesis, eventually assisted by microwave heating. During the past decade, several $Al(OH)_3$-*amine*-$HF_{aq.}$-ethanol systems were investigated over large concentration domains [8–13]. Numerous new hybrid fluorides were evidenced and an exceptional number of phases were found in the system with *tren* (tris-(2-aminoethyl)amine). Apart from 3D, all inorganic dimensionalities with various sizes of inorganic polyanions were observed. Consequently, our current research is focused on the synthesis of high valence metal fluorides associated with *tren* by low temperature evaporation, as reported by Bauer et al. [14], or solvothermal reaction at 190 °C. It is expected that high cation charge and high coordination favour the formation of large polyanions and that their condensation to give a three-dimensional inorganic framework can be achieved, as observed in $(H_3O)\cdot[Hgua]_5\cdot(ZrF_5)_6$. The ZrF_4-*tren*-$HF_{aq.}$-ethanol system was then chosen. Isolated metal fluoride anions appeared in $[H_3tren]\cdot(ZrF_7)_2\cdot 9H_2O$ [15] and the condensation of metal fluoride anions was only observed in $[H_3tren]\cdot(ZrF_6)\cdot(Zr_2F_{12})$ and $[H_4tren]\cdot(Zr_3F_{16}(H_2O))$ [16]. The Ta^V Ta_2O_5-*tren*-$HF_{aq.}$-ethanol system was also selected preferentially to other M^V (V_2O_5, Nb_2O_5)-*tren*-$HF_{aq.}$-ethanol systems; it is known that vanadium or niobium are prone to build numerous oxide–fluoride polyanions [17]. Isolated metal fluoride anions were evidenced in $[H_4tren]\cdot(TaF_7)_2\cdot H_2O$ and $[H_4tren]\cdot(TaF_7)_2$ [18].

This paper presents the composition space diagram of the ZrF_4-*tren*-$HF_{aq.}$-ethanol system at 190 °C over extended concentration ranges. Four new fluoride zirconates are found: α- and β-$[H_4tren]\cdot(Zr_2F_{12})$, $[H_4tren]\cdot(Zr_2F_{12})\cdot H_2O$ at high HF concentration

* Corresponding author. Tel.: +33 2 4383 3346; fax: +33 2 4383 3506.
E-mail address: annie.ribaud@univ-lemans.fr (A. Hémon-Ribaud).

0022-1139/$ – see front matter © 2011 Elsevier B.V. All rights reserved.
doi:10.1016/j.jfluchem.2011.05.007

and $[H_3tren]_4{\cdot}(ZrF_8)_3{\cdot}4H_2O$ at lower HF concentration. In the Ta_2O_5-*tren*-$HF_{aq.}$-ethanol system at 190 °C, only one oxide–fluoride polyanion is found in two varieties of $[H_3tren]_2{\cdot}(Ta_3O_2F_{16}){\cdot}(F)$.

2. Results and discussion

The ZrF_4-*tren*-$HF_{aq.}$-EtOH and Ta_2O_5-*tren*-$HF_{aq.}$-EtOH systems were first investigated in Teflon-lined Paar autoclaves with an external heating (2–3 days). Two zirconium fluorides were evidenced in ZrF_4 and *tren* rich solutions, together with one tantalum fluoride [16]. In the same time, it was shown that reaction and crystal growth kinetics in hydrothermal or solvothermal solutions are greatly fastened with microwave heating. The syntheses can be performed in 1 h and the crystal size is sufficient for single crystal diffraction experiments. This method was then applied to the previous zirconium system over the HF rich part of the system and over larger concentration domains. Four new zirconium fluorides appeared. For a reason of cost, the tantalum system was further studied in smaller Paar autoclaves in HF and *tren* rich concentrations and three new tantalum fluorides were evidenced.

2.1. ZrF_4-tren-$HF_{aq.}$-EtOH system composition space diagram

The composition space diagram of the ZrF_4-*tren*-$HF_{aq.}$-EtOH system is established for a constant concentration $[Zr^{4+}] = 0.5$ mol L^{-1} at 190 °C. Every experiment was performed during 1 h under microwave heating. The results are shown in a triangular representation, as already reported in [19,20] (Fig. 1). The labels are located at the representative points of the starting compositions and they are only indicative of the nature of the crystallized solids. Crystallization zones are approximately delimited; they overlap strongly and pure phases are not obtained. Then, thermogravimetric and chemical analyses cannot be performed. Eleven hybrid phases are evidenced; four compounds were previously described, four new phases are evidenced (this paper). Three extra phases are not yet identified (P_1, P_2 and P_3): single phases cannot be obtained and no structural characterisation is possible (tables of inter-reticular distances are given as Supplementary Materials). The optimal conditions for the synthesis of the eight identified hybrid fluorides are indicated in Table 1.

At the highest HF concentrations and low amine concentration, the zirconium species condense into dimeric polyanions and the amine is tetraprotonated. Three phases appear and present close structural analogies: $[H_4tren]{\cdot}(Zr_2F_{12}){\cdot}H_2O$ (**1**), α-$[H_4tren]{\cdot}(Zr_2F_{12})$ (**2**) and β-$[H_4tren]{\cdot}(Zr_2F_{12})$ (**3**). When the [HF]/[ZrF_4] ratio decreases, at low amine concentration, the zirconium species condense into infinite chains in $[H_4tren]{\cdot}(Zr_3F_{16}(H_2O))$ [16].

At low HF concentration and high amine concentration, $[H_3tren]_2{\cdot}(ZrF_7)_2{\cdot}9H_2O$ exists over a large domain. $[H_3tren]_2{\cdot}(ZrF_7)_2{\cdot}H_2O$ and $[H_3tren]_4{\cdot}(ZrF_8)_3{\cdot}4H_2O$ (**4**) coexist in very similar concentrations $1 < [tren]/[ZrF_4] < 4$ and $2 < [HF]/[ZrF_4] < 18$. All three previous phases are built up from triprotonated $[H_3tren]^{3+}$ cations and isolated anions, $(ZrF_7)^{3-}$ or $(ZrF_8)^{4-}$. $[H_3tren]_2{\cdot}(ZrF_7)_2{\cdot}H_2O$ results also from the dehydration of $[H_3tren]_2{\cdot}(ZrF_7)_2{\cdot}9H_2O$ at 90 °C under argon atmosphere [15].

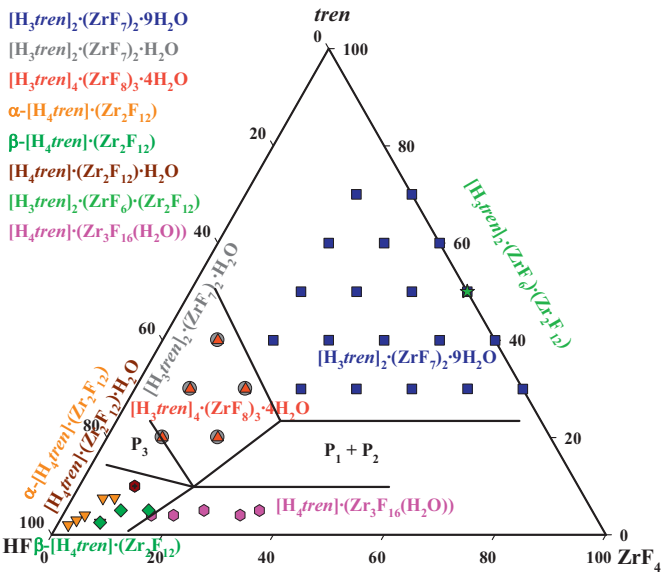

Fig. 1. Composition space representation of the ZrF_4-*tren*-$HF_{aq.}$-EtOH system.

In the absence of HF, $[H_3tren]{\cdot}(ZrF_6){\cdot}(Zr_2F_{12})$ is found on the ZrF_4-*tren* line [16].

It is clear that tetraprotonation of the amine occurs only at very high HF concentration. Moreover, the inorganic dimensionality increases at low amine concentration and the ratio *tren*/F in the solids is in agreement with the variation of amine and fluoride concentrations in the starting mixtures.

2.2. Ta_2O_5-tren-$HF_{aq.}$-EtOH system

The composition space diagram of the Ta_2O_5-*tren*-$HF_{aq.}$-EtOH system at 190 °C was already published in [11]. Four fluoride or oxide–fluoride tantalates of $[H_3tren]^{3+}$ crystallise: $[H_3tren]{\cdot}(TaF_7){\cdot}(F)$, described in [16], one phase that is supposed to be $[H_3tren]_2{\cdot}(Ta_2F_{13})_2{\cdot}H_2O$ and two varieties of $[H_3tren]_2{\cdot}(Ta_3O_2F_{16}){\cdot}(F)$. These last varieties are described here. The optimal conditions for the synthesis are indicated in Table 1.

The tetraprotonation of the amine does not occur, even at high HF concentrations. The result is opposite when the same starting compositions are left for evaporation at 40 °C: $[H_4tren]{\cdot}(TaF_7){\cdot}H_2O$ or $[H_4tren]{\cdot}(TaF_7){\cdot}H_2O$ appear [18].

Table 1
Optimal synthesis conditions of *tren*-based fluoride zirconates and tantalates.

Formulation	Inorganic (poly)anions or chains	Molar ratio, ZrF_4/*tren*/HF/EtOH	Reference
$[H_3tren]_2{\cdot}(ZrF_7)_2{\cdot}9H_2O$	$(ZrF_7)^{3-}$	0.5/0.67/0.5/17	[15]
$[H_3tren]_2{\cdot}(ZrF_7)_2{\cdot}H_2O$	$(ZrF_7)^{3-}$	0.5/2/2.5/17	[15]
$[H_4tren]{\cdot}(Zr_2F_{12}){\cdot}H_2O$ **(1)**	$(Zr_2F_{12})^{4-}$	0.5/0.5/4/17	This work
α-$[H_4tren]{\cdot}(Zr_2F_{12})$ **(2)**	$(Zr_2F_{12})^{4-}$	0.5/0.25/4.25/17	This work
β-$[H_4tren]{\cdot}(Zr_2F_{12})$ **(3)**	$(Zr_2F_{12})^{4-}$	0.5/0.5/15.5/17	This work
$[H_3tren]_4{\cdot}(ZrF_8)_3{\cdot}4H_2O$ **(4)**	$(ZrF_8)^{4-}$	0.5/1/3.5/17	This work
$[H_3tren]_2{\cdot}(ZrF_6){\cdot}(Zr_2F_{12})$	$(ZrF_6)^{2-}$, $(Zr_2F_{12})^{4-}$	0.5/0.5/0/17	[16]
$[H_4tren]{\cdot}(Zr_3F_{16}(H_2O))$	$_\infty(Zr_3F_{16}(H_2O))^{4-}$	0.5/0.1/1.4/17	[16]
$[H_3tren]{\cdot}(TaF_7){\cdot}(F)$	$(TaF_7)^{2-}$	0.2/0.06/1/17	[16]
$[H_3tren]_2{\cdot}(Ta_2F_{13})_2{\cdot}H_2O$	$(Ta_2F_{13})^{3-}$	0.2/0.2/7.6/17	[11]
α-$[H_3tren]_2{\cdot}(Ta_3O_2F_{16}){\cdot}(F)$ **(5)**	$(Ta_3O_2F_{16})^{5-}$	0.2/0.28/0.36/17	This work
β-$[H_3tren]_2{\cdot}(Ta_3O_2F_{16}){\cdot}(F)$ **(6)**	$(Ta_3O_2F_{16})^{5-}$	0.2/0.3/0.15/17	This work

Table 2
Crystallographic data of $[H_4tren]\cdot(Zr_2F_{12})\cdot H_2O$ (**1**), α-$[H_4tren]\cdot(Zr_2F_{12})$ (**2**), β-$[H_4tren]\cdot(Zr_2F_{12})$ (**3**), $[H_3tren]_4\cdot(ZrF_8)_3\cdot 4H_2O$ (**4**), α-$[H_3tren]_2\cdot(Ta_3O_2F_{16})\cdot(F)$ (**5**) and β-$[H_3tren]_2\cdot(Ta_3O_2F_{16})\cdot(F)$ (**6**).

Compound	(1)	(2)	(3)	(4)	(5)	(6)
Formula weight ($g\,mol^{-1}$)	578.70	560.69	560.69	1397.91	882.13	882.13
Crystal size (mm^3)	$0.20\times0.18\times0.18$	$0.06\times0.11\times0.30$	$0.22\times0.06\times0.04$	$0.14\times0.14\times0.15$	$0.03\times0.10\times0.10$	$0.06\times0.10\times0.10$
Crystal system	Orthorhombic	Orthorhombic	Monoclinic	Cubic	Monoclinic	Rhomboedral
Space group	$P2_12_12_1$	$P2_12_12_1$	$P2_1/c$	$I23$	$C2/m$	$R32$
a (Å)	8.6130(4)	8.1211(9)	13.5748(9)	13.66(1)	15.527(6)	8.834(9)
b (Å)	13.3477(8)	12.874(3)	9.8430(6)		8.765(5)	
c (Å)	15.0733(7)	15.195(1)	11.8546(7)		14.65(2)	31.704(4)
Angle (°)			$\beta=97.187(3)$		$\beta=134.24$ (3)	$\gamma=120$
V ($Å^3$), Z	1732.9(3), 4	1588.6(7), 4	1571.5(3), 4	2549(2), 2	1428(2), 2	2142(1), 3
$\rho_{calc.}$ ($g\,cm^{-3}$)	2.22	2.35	2.37	1.83	2.80	2.80
μ (mm^{-1})	1.33	1.44	1.46	0.74	11.60	11.60
2θ range (°)	4–60	3–60	3–103	4–70	5–55	5–70
T_{min}, T_{max}	0.78, 0.80	0.83, 0.92	0.74, 0.94	0.89, 0.91	0.37, 0.71	0.07, 0.51
Secondary extinction	–	–	–	$0.5(2)\times10^{-5}$	–	
$h\,k\,l$	$\lvert h\rvert\le12$	$\lvert h\rvert\le11$	$\lvert h\rvert\le29$	$\lvert h\rvert\le13$	$\lvert h\rvert\le20$	$-9\le h\le11$
	$\lvert k\rvert\le18$	$\lvert k\rvert\le18$	$\lvert k\rvert\le21$	$\lvert k\rvert\le13$	$\lvert k\rvert\le11$	$\lvert k\rvert\le13$
	$\lvert l\rvert\le21$	$\lvert l\rvert\le21$	$-24\le l\le26$	$\lvert l\rvert\le19$	$\lvert l\rvert\le19$	$\lvert l\rvert\le51$
Refl. meas./unique/($I>2\sigma(I)$)	17847/5025/4707	5300/4607/3523	112487/17280/10127	1653/1086/850	3490/1713/1037	50301/1815/1481
Refined parameters (on F^2)	237	221	221	58	108	77
R(int)/R(sigma)	0.057/0.049	0.044/0.072	0.040/0.036	–/0.045	0.112/0.125	0.044/0.032
R_1/wR_2	0.037/0.093	0.048/0.11	0.035/0.092	0.073/0.21	0.065/0.175	0.047/0.14
Goodness of fit	1.03	1.09	1.03	1.09	1.02	0.98
Flack parameter	−0.10(4)	−0.18(7)		0.05(23)		0.51(6)
$\Delta\rho_{min}/\Delta\rho_{max}$ ($e\,Å^{-3}$)	−0.98/1.74	−0.66/0.91	−0.72/1.82	−0.70/1.26	−2.46/3.04	−4.46/4.28

Crystallographic data (excluding structure factors) for the structures have been deposited with the Cambridge Crystallographic Data Center as supplementary publication nos. CCDC 824421 (**1**), CCDC 824422 (**2**), CCDC 824423 (**3**), CCDC 824424 (**4**), CCDC 824425 (**5**) and CCDC 824426 (**6**). Copies of data can be obtained, free of charge, on application to CCDC, 12 Union Road, Cambridge CB2 1EZ, UK (fax: +44 1223 336033 or deposit@ccdc.cam.ac.uk).

2.3. Structure descriptions and discussion

2.3.1. Zr_2F_{12} dimers in $[H_4tren]\cdot(Zr_2F_{12})\cdot H_2O$ (1), α-$[H_4tren]\cdot(Zr_2F_{12})$ (2) and β-$[H_4tren]\cdot(Zr_2F_{12})$ (3)

Crystallographic data and the conditions of data collection are indicated in Table 2. The structures of $[H_4tren]\cdot(Zr_2F_{12})\cdot H_2O$ (**1**), α-$[H_4tren]\cdot(Zr_2F_{12})$ (**2**) and β-$[H_4tren]\cdot(Zr_2F_{12})$ (**3**) are represented in Figs. 2 and 3. They are built up from $(Zr_2F_{12})^{4-}$ dimers in which two ZrF_7 distorted pentagonal bipyramids (1:5:1 coordination) are linked by a common edge (Fig. 4, left). The Zr–F distances lie in the range 2.13–2.22 Å for bridging fluorine atoms and 1.95–2.08 Å for non-bridging fluorine atoms (Table 3). $[H_4tren]^{4+}$ cations adopt planar or "scorpion" type configurations indicative of the protonation state [11] (Fig. 5, left). They exchange hydrogen

Table 3
Selected inter-atomic distances (Å) in $[H_4tren]\cdot(Zr_2F_{12})\cdot H_2O$ (1), α-$[H_4tren]\cdot(Zr_2F_{12})$ (2) and β-$[H_4tren]\cdot(Zr_2F_{12})$ (3).

$[H_4tren]\cdot(Zr_2F_{12})\cdot H_2O$		α-$[H_4tren]\cdot(Zr_2F_{12})$		β-$[H_4tren]\cdot(Zr_2F_{12})$	
Zr(1)–F(10)	1.980(3)	Zr(1)–F(12)	1.948(5)	Zr(1)–F(1)	1.990(1)
Zr(1)–F(12)	1.996(3)	Zr(1)–F(9)	1.998(4)	Zr(1)–F(3)	2.013(1)
Zr(1)–F(9)	2.012(2)	Zr(1)–F(10)	1.999(4)	Zr(1)–F(2)	2.016(1)
Zr(1)–F(7)	2.051(2)	Zr(1)–F(7)	2.027(4)	Zr(1)–F(4)	2.054(1)
Zr(1)–F(6)	2.061(2)	Zr(1)–F(6)	2.050(4)	Zr(1)–F(5)	2.073(1)
Zr(1)–F(1)	2.165(2)	Zr(1)–F(1)	2.166(4)	Zr(1)–F(6)	2.173(1)
Zr(1)–F(2)	2.183(2)	Zr(1)–F(2)	2.225(4)	Zr(1)–F(6)	2.192(1)
⟨Zr(1)–F⟩	2.06	⟨Zr(1)–F⟩	2.06	⟨Zr(1)–F⟩	2.07
Zr(2)–F(11)	1.987(3)	Zr(2)–F(5)	1.977(4)	Zr(2)–F(8)	2.009(1)
Zr(2)–F(5)	1.994(3)	Zr(2)–F(11)	1.998(5)	Zr(2)–F(7)	2.013(1)
Zr(2)–F(8)	2.041(2)	Zr(2)–F(4)	2.036(4)	Zr(2)–F(9)	2.019(1)
Zr(2)–F(4)	2.041(2)	Zr(2)–F(8)	2.041(4)	Zr(2)–F(10)	2.020(1)
Zr(2)–F(3)	2.065(2)	Zr(2)–F(3)	2.074(4)	Zr(2)–F(11)	2.083(1)
Zr(2)–F(1)	2.143(2)	Zr(2)–F(1)	2.131(4)	Zr(2)–F(12)	2.166(1)
Zr(2)–F(2)	2.175(2)	Zr(2)–F(2)	2.168(4)	Zr(2)–F(12)	2.186(1)
⟨Zr(2)–F⟩	2.06	⟨Zr(2)–F⟩	2.06	⟨Zr(2)–F⟩	2.07
N(1)–C(1)	1.487(5)	N(1)–C(1)	1.494(8)	N(1)–C(1)	1.505(2)
N(1)–C(5)	1.503(5)	N(1)–C(5)	1.495(8)	N(1)–C(5)	1.518(2)
N(1)–C(3)	1.512(5)	N(1)–C(3)	1.498(8)	N(1)–C(3)	1.518(2)
N(2)–C(2)	1.476(5)	N(2)–C(2)	1.467(9)	N(3)–C(4)	1.484(2)
N(3)–C(4)	1.505(4)	N(3)–C(4)	1.493(9)	N(4)–C(6)	1.487(2)
N(4)–C(6)	1.467(5)	N(4)–C(6)	1.491(8)	N(2)–C(2)	1.492(2)
N(1)–N(2)	3.774(5)	N(1)–N(2)	3.753(7)	N(1)–N(2)	3.791(2)
N(1)–N(3)	3.829(5)	N(1)–N(3)	3.813(7)	N(1)–N(3)	3.305(2)
N(1)–N(4)	3.780(5)	N(1)–N(4)	3.175(7)	N(1)–N(4)	3.813(2)
C(3)–C(4)	1.517(5)	C(3)–C(4)	1.511(8)	C(5)–C(6)	1.520(2)
C(5)–C(6)	1.515(5)	C(5)–C(6)	1.523(9)	C(1)–C(2)	1.521(2)
C(1)–C(2)	1.524(6)	C(1)–C(2)	1.529(9)	C(3)–C(4)	1.529(2)
Ow–F(5)	2.655(5)				
Ow–F(7)	2.658(5)				

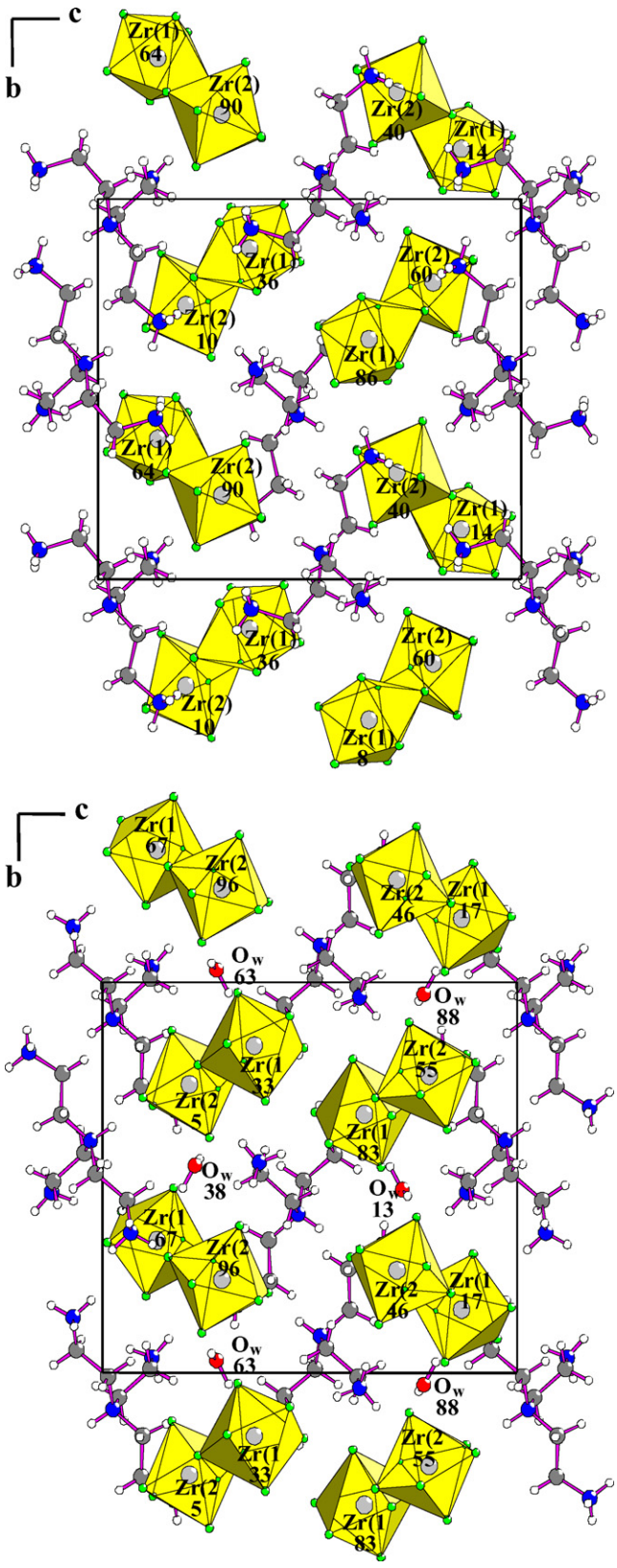

Fig. 2. [1 0 0] projections of α-[H_4tren]·(Zr_2F_{12}) (**2**) (top) and [H_4tren]·(Zr_2F_{12})·H_2O (**1**) (bottom).

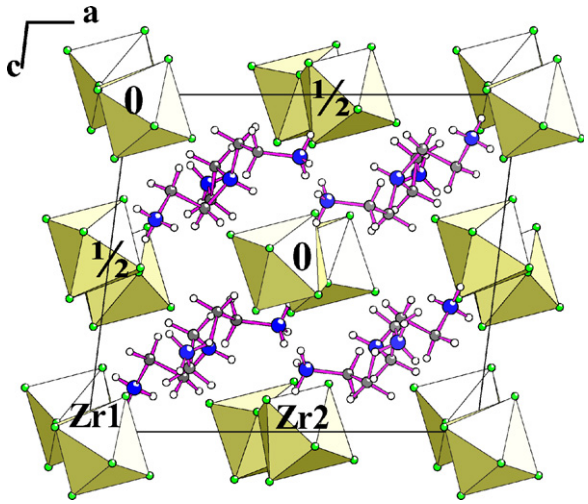

Fig. 3. [0 1 0] projection of β-[H_4tren]·(Zr_2F_{12}) (**3**).

bonds with fluorine atoms from seven dimers in (**1**) and (**2**) and from eight dimers in (**3**). Two water molecules are also hydrogen bonded with $[H_4tren]^{4+}$ cation in (**1**).

[H_4tren]·(Zr_2F_{12})·H_2O (**1**) and α-[H_4tren]·(Zr_2F_{12}) (**2**) are described in the same $P2_12_12_1$ space group and their cell parameters are very similar (Table 2). Apart from H_2O molecule, the atomic parameters (*-x*, *-y*, *-z* in (**1**)) are roughly similar also (see Supplementary Materials). These features are evidenced by the [1 0 0] projections of the structures (Fig. 2). In the hydrated phase, a water molecule is connected by strong hydrogen bonds to two fluoride anions of two different dimers (F···H–Ow, 2.65–2.66 Å) (Fig. 5, left).

In β-[H_4tren]·(Zr_2F_{12}) (**3**), the $(Zr_2F_{12})^{4-}$ dimers are centered on the origin (0 0 0) and three other equivalent symmetry centers (Fig. 3). It must be noted that such isolated dimers are not very frequently encountered in hybrid fluorides [21–25].

2.3.2. ZrF_8 dodecahedra in [H_3tren]$_4$·(ZrF_8)$_3$·$4H_2O$ (4)

The structure of [H_3tren]$_4$·(ZrF_8)$_3$·$4H_2O$ is cubic. Zirconium atoms exhibit an eight-fold coordination in a slightly distorted ZrF_8 dodecahedron (Fig. 4, right); the polyhedron symmetry is 222 and the Zr–F distances are in the range 2.05–2.09 Å (Table 4). [H_3tren]$_4$·(ZrF_8)$_3$·$4H_2O$ is the first hybrid fluoride with this eight-fold coordination. Only one example exists in the inorganic fluoride $Li_6BeF_4ZrF_8$ in which the dodecahedron symmetry is $\bar{4}m2$ [26]. *Tren* amines are triprotonated and adopt a "spider" configuration [11]. The central tertiary nitrogen atoms of amines and O_w oxygen atoms of water molecules are located on three fold symmetry axes (Figs. 5 (right) and 6). Water molecule is hydrogen bonded to three terminal NH_3^+ groups of one amine (O_w···H–$N_{primary}$, 2.73 Å). Nine strong hydrogen bonds are established between three terminal NH_3 groups of $[H_3tren]^{3+}$ cation and fluoride anions of six ZrF_8 polyhedra (F···H–$N_{primary}$, 2.80–2.86 Å).

Table 4
Selected inter-atomic distances (Å) in [H_3tren]$_4$·(ZrF_8)$_3$·$4H_2O$ (**4**).

Zr–F(1)	4 × 2.049(9)	N(1)–C(1)	3 × 1.49(1)
Zr–F(2)	4 × 2.092(9)	C(1)–C(2)	1.52(1)
⟨Zr–F⟩	2.07	C(2)–N(2)	1.42(1)
O_w(1)–N(1)	3.16(1)	N(1)–N(2)	3 × 2.98(1)
O_w(1)–N(2)	3 × 2.73(1)	N(2)–N(2)	3 × 4.10(1)
F(1)–N(2)	3 × 2.80(1)		
F(1)–N(2)	3 × 2.83(1)		
F(2)–N(2)	3 × 2.86(1)		

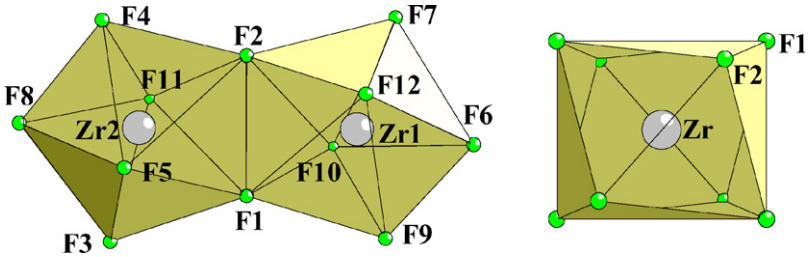

Fig. 4. $(Zr_2F_{12})^{4-}$ dimer in α-[H_4*tren*]·(Zr_2F_{12}) (**2**) (left) and ZrF_8 polyhedron in [H_3*tren*]$_4$·(ZrF_8)$_3$·4H_2O (**4**) (right).

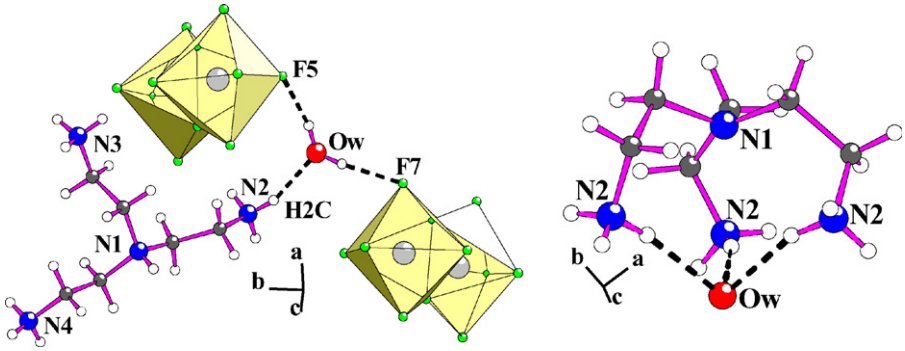

Fig. 5. Hydrogen bonding of water molecules in [H_4*tren*]·(Zr_2F_{12})·(H_2O) (**1**) (left) and [H_3*tren*]$_4$·(ZrF_8)$_3$·4H_2O (**4**) (right).

2.3.3. α,β-[H_3*tren*]$_2$·($Ta_3O_2F_{16}$)·(F) (**5**, **6**)

The structure determinations of the α and β varieties of [H_3*tren*]$_2$·($Ta_3O_2F_{16}$)·(F) are difficult. A disorder affects either the organic or the inorganic parts and, consequently, average structures are only proposed here. [H_3*tren*]$_2$·($Ta_3O_2F_{16}$)·(F) crystallises in a rhomboedral β form (**6**) and its monoclinic distortion, the α form (**5**) (Table 2).

A large cell is found for the β form: a_H = 15.30 Å, c_H = 31.70 Å. However, the existence conditions on the reflections $(h\,0\,\bar{h}\,0)$, $h = 6n$ and $(0\,k\,\bar{k}\,0)$, $k = 6n$ are not compatible with any space group conditions. A twinning is then responsible of these pseudo-conditions and no structure solution can be obtained with such a hypothesis. It is observed that very few weak reflections imply the previous large cell and that a smaller rhombohedral cell with a_H = 8.83 Å and c_H = 31.70 Å can be deduced if these reflections are omitted. The existence conditions are then compatible with the centrosymmetric $R\bar{3}m$ space group. However, a structure solution appears only in the $R\bar{3}$ space group. The crystallographic positions of Ta(1), Ta(2), five fluorine or oxygen atoms, two carbon atoms and two nitrogen atoms are found with very high thermal motion parameters (R_1 = 0.061). Finally, a better solution is found in *R*32 space group (R_1 = 0.047); Ta(1), Ta(2), F(1), oxygen atoms and the amine groups are well localised but a disorder remains on F(2) and F(3). Taking into account the site occupancies, this solution suggests the formulation [H_3*tren*]$_2$·($Ta_3O_2F_{16}$)·(F). The absolute structure cannot be determined reliably.

Similar difficulties due to disorder were also encountered during the determination of the structure of α-[H_3*tren*]$_2$·($Ta_3O_2F_{16}$)·(F). The cell is monoclinic and the reflection conditions are consistent with the *C*2/*m* space group. The relation between this monoclinic cell and the small rhombohedral cell (hexagonal axes) of the β form is characterized by $V_{mono} = \frac{2}{3}V_{hex}$ and the following axes transformations: $\vec{a}_{hex} = (\vec{a}_{mono} - \vec{b}_{mono})/2$, $\vec{b}_{hex} = \vec{b}_{mono}$, $\vec{c}_{hex} = 3\vec{c}_{mono} + 2\vec{a}_{mono}$. Ta(1), Ta(2), two fluorine or oxygen atoms and three nitrogen atoms are localised with full site occupancies but a disorder remains on carbon atoms and the remaining fluorine atoms. The suggested formulation is also [H_3*tren*]$_2$·($Ta_3O_2F_{16}$)·(F).

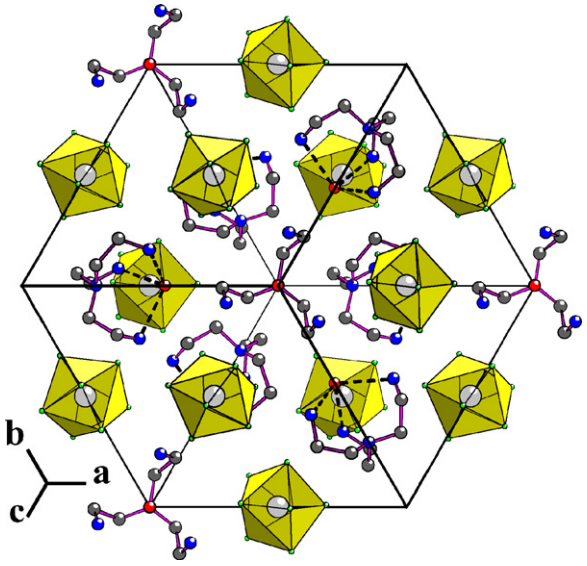

Fig. 6. [1 1 1] projection of the structure of [H_3*tren*]$_4$·(ZrF_8)$_3$·4H_2O (**4**).

The projections of the structures appear in Fig. 7. Both compounds are built up from $[H_3tren]^{3+}$ cations, isolated F^- anions and isolated $Ta_3O_2F_{16}$ trimers. The trimers result from the linear connection of two $(TaOF_6)^{3-}$ pentagonal bipyramids to a central $(TaO_2F_4)^{3-}$ octahedron by opposite oxygen corners. All atoms in axial positions are well localised and only the equatorial fluorine atoms are disordered. "Free" fluoride ion is octahedrally surrounded by six $-NH_3^+$ groups of two $[H_3tren]^{3+}$ cations with a "spider" shape (Fig. 7, right). Such an environment was already found in [H_3*tren*]$_4$·(AlF_6)$_2$·(Al_2F_{11})·(F)·10H_2O [11,13].

The similarity of the α and β phases and the distortion of the α phase are confirmed by the X-ray powder patterns (Fig. 8). NMR experiments were performed in order to confirm the presence of "free" fluoride ions. However, the interpretation of the spectra is not conclusive; the chemical shifts from "free" fluoride ions cannot

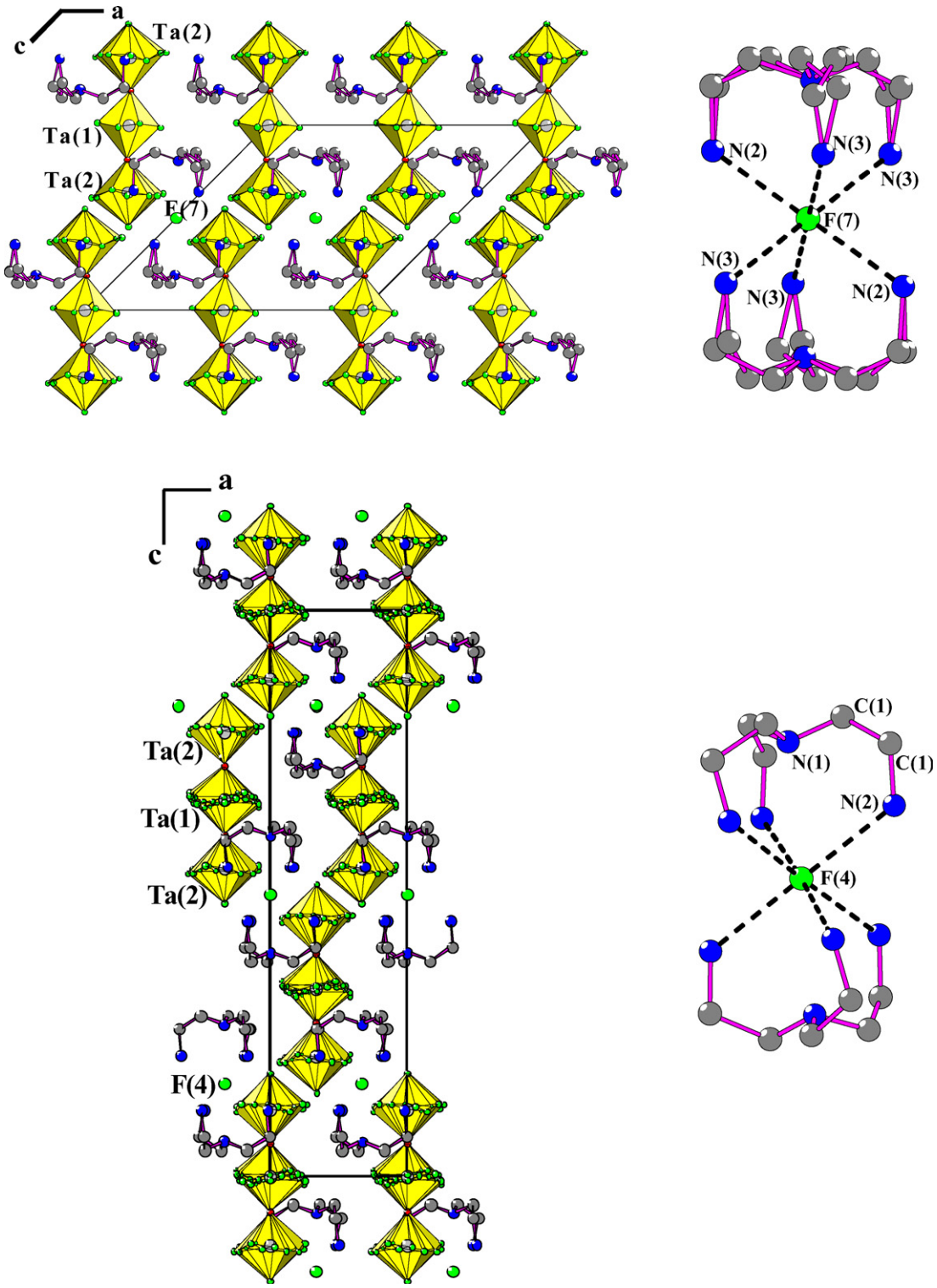

Fig. 7. [0 1 0] projection (top, left) and view of octahedral environment of free fluoride F(7) ion (top, right) in α-[H_3*tren*]$_2$·($Ta_3O_2F_{16}$)$_3$·(F) (**5**); [0 1 0] projection (bottom, left) and view of environment of F(4) free fluoride ion (bottom, right) in β-[H_3*tren*]$_2$·($Ta_3O_2F_{16}$)$_3$·(F) (**6**).

be distinguished from that of tantalum-bonded fluorine atoms [11,27].

3. Conclusion

Six new fluoride zirconates or tantalates are evidenced in the (ZrF_4 or Ta_2O_5)-*tren*-$HF_{aq.}$-ethanol systems at 190 °C. Two varieties α and β of [H_4*tren*]·(Zr_2F_{12}) and of [H_3*tren*]$_2$·($Ta_3O_2F_{16}$)·(F) appear. They are built up from $(Zr_2F_{12})^{4-}$ dimers, together with [H_4*tren*]·(Zr_2F_{12})·H_2O, and from $(Ta_3O_2F_{16})^{5-}$ trimers, respectively. The trimers were unknown in the chemistry of tantalates, as well as the dodecahedral unit ZrF_8 of [H_3*tren*]$_4$·(ZrF_8)$_3$·4H_2O in hybrid fluoride zirconates. While both varieties of [H_4*tren*]·(Zr_2F_{12}) do not have any evident structure relationship, α-[H_3*tren*]$_2$·($Ta_3O_2F_{16}$)·(F) is a simple monoclinic distortion of β-[H_3*tren*]$_2$·($Ta_3O_2F_{16}$)·(F). It would be interesting to analyse the reasons of this phase allotropy

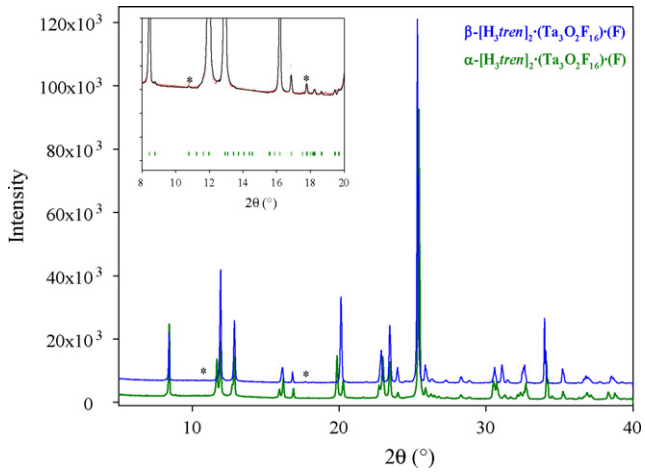

Fig. 8. Comparison of the diffraction patterns of α-$[H_3tren]_2{\cdot}(Ta_3O_2F_{16}){\cdot}(F)$ (**5**) and β-$[H_3tren]_2{\cdot}(Ta_3O_2F_{16}){\cdot}(F)$ (**6**): evidence of the monoclinic distortion for α-$[H_3tren]_2{\cdot}(Ta_3O_2F_{16}){\cdot}(F)$ and of the diffraction lines (noted by *) responsible of the large primitive cell of β-$[H_3tren]_2{\cdot}(Ta_3O_2F_{16}){\cdot}(F)$. The insert is an enlargement of the low angle part of the diffraction pattern.

and, particularly, to examine the role of small variations of the HF concentrations in the starting mixtures on eventual OH^-/F^- substitutions in the solids.

4. Experimental

All phases were synthesized from a mixture of ZrF_4 (UltraFluor) or Ta_2O_5 (Alfa Aesar), hydrofluoric acid solution (48% HF, Prolabo), tris-(2-aminoethyl)amine (*tren*) (Aldrich) and ethanol (EtOH). With ZrF_4, the solvothermal reactions were performed at 190 °C in Teflon autoclaves during 1 h in a microwave oven (CEM MDS 2100); with Ta_2O_5, Parr autoclaves were heated during 48 h at 190 °C. The solid products were washed with ethanol and dried at room temperature. Phase purity was confirmed by the comparison of observed and simulated X-ray powder diffraction patterns. Single crystals were obtained and X-ray diffraction data were collected with a Bruker Kappa CCD area-detector diffractometer (**1**, **3**, **6**) or a SIEMENS AED2 four-circle diffractometer (ω–2θ scans) (**2**, **4**, **5**). The structures were determined with direct methods using SHELXS-97 program [28], extended by successive difference Fourier syntheses and refined with least-squares minimisation techniques against F^2 using SHELXL-97 [29] in WinGX package [30]. The nature of the atoms was distinguished from distance criteria [31]. Thermal motions of all non-hydrogen and non-disordered atoms were refined anisotropically. Hydrogen atoms of non-disordered amine cations were localized from geometrical constraint conditions, which imply equal distances and angles to the central atom (HFIX option) whereas the O–H distances and H–O–H angles of water molecules were fixed using the DFIX option. The absolute configurations of the non-centrosymmetric structures (**1**, **2** and **4**) are proposed by using the Flack absolute structure parameter [32]. In $[H_3tren]_4{\cdot}(ZrF_8){\cdot}4H_2O$ (**4**), the hydrogen atoms of water molecules were not localized.

Conditions of data collection, crystallographic data and structural refinements are summarised in Table 2. The resulting atomic coordinates with equivalent anisotropic displacement parameters (ADP) are given in Supplementary Materials; several selected interatomic distances appear respectively in Tables 3–6. Structure projections are drawn with the DIAMOND program [33].

Table 5
Selected inter-atomic distances (Å) in α-$[H_3tren]_2{\cdot}(Ta_3O_2F_{16}){\cdot}(F)$ (**5**).

Ta(1)–F(5)	2 × 1.85(2)	Ta(2)–F(1a)	1.81(3)
Ta(1)–F(6)	2 × 1.89(2)	Ta(2)–O	1.83(2)
Ta(1)–O	2 × 1.97(2)	Ta(2)–F(4)	0.33 × 1.92(3)
		Ta(2)–F(2b)	1.92(3)
N(1)–C(4b)	1.42(5)	Ta(2)–F(3)	1.95(1)
N(1)–C(4a)	1.52(4)	Ta(2)–F(2c)	0.33 × 1.96(4)
N(1)–C(1)	1.52(3)	Ta(2)–F(1b)	2.02(3)
		Ta(2)–F(2a)	2.02(3)
N(2)–C(2)	1.53(4)	Ta(2)–F(4b)	0.33 × 2.05(3)
N(3)–C(3a)	1.40(4)		
N(3)–C(3b)	1.57(4)	N(2)–N(3)	2 × 4.18(4)
		N(3)–N(3)	3.89(4)
		N(1)–N(3)	2 × 2.92(2)
		N(1)–N(2)	2.99(5)
C(1)–C(2)	1.49(5)	N(3)–F(7)	4 × 2.85(2)
C(3a)–C(4a)	1.49(6)	N(2)–F(7)	2 × 2.87(2)

Table 6
Selected inter-atomic distances (Å) in β-$[H_3tren]_2{\cdot}(Ta_3O_2F_{16}){\cdot}(F)$ (**6**).

Ta(1)–F(3b)	1.89(2)	Ta(2)–O	1.87(1)
Ta(1)–F(3a)	1.93(3)	Ta(2)–F(2e)	1.88(3)
Ta(1)–O	2 × 1.93(1)	Ta(2)–F(2d)	1.90(2)
Ta(1)–F(3d)	1.94(2)	Ta(2)–F(2c)	1.91(2)
Ta(1)–F(3c)	2.08(3)	Ta(2)–F(2a)	1.96(2)
		Ta(2)–F(1)	2.02(1)
		Ta(2)–F(2b)	2.04(2)
N(1)–C(1)	3 × 1.45(1)	N(1)–N(2)	3 × 2.95(1)
C(1)–C(2)	1.55(1)	N(2)–N(2)	3 × 4.14(2)
N(2)–C(2)	1.48(1)	N(2)–F(4)	6 × 2.84(1)

Acknowledgements

Thanks are due to the "Institut Français de Coopération" (Tunisia) for a Ph.D. grant (M.A. Saada).

Appendix A. Supplementary data

Supplementary data associated with this article can be found, in the online version, at doi:10.1016/j.jfluchem.2011.05.007.

References

[1] P. Horcajada, T. Chalati, C. Serre, B. Gillet, C. Sebrie, T. Baati, J.F. Eubank, D. Heurtaux, P. Clayette, C. Kreuz, J.-S. Chang, Y.K. Hwang, V. Marsaud, P.-N. Bories, L. Cynober, S. Gil, G. Férey, P. Couvreur, R. Gref, Nat. Mater. 9 (2010) 172–178.
[2] P.L. Llewellyn, S. Bourrelly, C. Serre, A. Vimont, M. Daturi, L. Hamon, G. De Weireld, J.-S. Chang, D.-Y. Hong, Y.K. Hwang, S.H. Jhung, G. Férey, Langmuir 24 (2008) 7245–7250.
[3] K. Adil, M. Leblanc, V. Maisonneuve, P. Lightfoot, Dalton Trans. 39 (2010) 5983–5993.
[4] L.A. Gerrard, M.T. Weller, Chem. Mater. 16 (2004) 1650–1659.
[5] P. Lightfoot, N.F. Stephens, Mater. Res. Soc. Symp. Proc. 848 (2005) 13–17.
[6] N.F. Stephens, P. Lightfoot, J. Solid State Chem. 180 (2007) 260–264.
[7] A.V. Gerasimenko, B.V. Bukvetskii, V.B. Logvinova, R.L. Davidovich, Koord. Khim. 22 (1996) 584–590.
[8] E. Goreshnik, M. Leblanc, V. Maisonneuve, Z. Anorg. Allg. Chem. 628 (2002) 162–166.
[9] K. Adil, M. Leblanc, V. Maisonneuve, Acta Crystallogr. E60 (2004) m1379–m1381.
[10] K. Adil, A. Ben Ali, M. Leblanc, V. Maisonneuve, Solid State Sci. 8 (2006) 698–703.
[11] K. Adil, M. Ali Saada, A. Ben Ali, M. Body, M. Trung Dang, A. Hémon-Ribaud, M. Leblanc, V. Maisonneuve, J. Fluorine Chem. 128 (2007) 404–412.
[12] K. Adil, J. Marrot, M. Leblanc, V. Maisonneuve, Solid State Sci. 9 (2007) 531–534.
[13] K. Adil, M. Leblanc, V. Maisonneuve, J. Fluorine Chem. 130 (2009) 1099–1105.
[14] M.R. Bauer, C.R. Ross II, R.M. Nielson, S.C. Abrahams, Inorg. Chem. 38 (1999) 1028–1030.
[15] M.A. Saada, A. Hémon-Ribaud, M. Leblanc, V. Maisonneuve, J. Fluorine Chem. 126 (2005) 1072–1077.
[16] E. Goreshnik, M. Leblanc, V. Maisonneuve, J. Solid State Chem. 177 (2004) 4023–4030.
[17] M. Gerken, H.P.A. Mercier, G. Schrobilgen, in: T. Nakajima, B. Zemva, A. Tressaud (Eds.), Advanced Inorganic Fluorides, Elsevier, Amsterdam, 2000 pp. 149–154 (Chapter 5).
[18] M.A. Saada, A. Hémon-Ribaud, M. Leblanc, V. Maisonneuve, J. Fluorine Chem. 126 (2005) 1246–1251.

[19] S.M. Walker, P.S. Halasyamani, S. Allen, D. O'Hare, J. Am. Chem. Soc. 121 (1999) 10513–10521.
[20] K. Adil, A. Le Bail, M. Leblanc, V. Maisonneuve, Inorg. Chem. 49 (2010) 2392–2397.
[21] I.P. Kondratyuk, M.F. Eiberman, R.L. Davidovich, M.A. Medkov, B.V. Bukvetskii, Koord. Khim. 7 (1981) 1109.
[22] B.V. Bukvetskii, A.V. Gerasimenko, I.P. Kondratyuk, R.L. Davidovich, M.A. Medkov, Koord. Khim. 13 (1987) 661.
[23] Y. Du, M. Yang, J. Yu, Q. Pan, R. Xu, Angew. Chem. Int. Ed. 44 (2005) 7988–7990.
[24] A. Ben Ali, L.S. Smiri, M. Leblanc, V. Maisonneuve, Jpn. Soc. Anal. Chem. 25 (2009) 37–38.
[25] I. Boldog, J.-C. Daran, A.N. Chernega, E.B. Rusanov, H. Krautscheid, K.V. Domasevitch, Cryst. Growth Des. 9 (2009) 2895–2905.
[26] D.R. Sears, J.H. Burns, J. Chem. Phys. 41 (1964) 3478–3483.
[27] M.A. Saada, Thesis, Université du Maine, 2006.
[28] G.M. Sheldrick, SHELXS-97": A Program for Automatic Solution of Crystal Structures, Göttingen University, Germany, 1997 (Release 97-2).
[29] G.M. Sheldrick, SHELXL-97": A Program for Crystal Structure Determination, Göttingen University, Germany, 1997.
[30] L.J. Farrugia, J. Appl. Cryst. 32 (1999) 837–838.
[31] R. Shannon, Acta Crystallogr. A 32 (1976) 751–767.
[32] H.D. Flack, Acta Crystallogr. A 39 (1983) 876–881.
[33] G. Bergerhoff, DIAMOND: Visual Crystal Structure Information System, Gerhard-Domagk-Str. 1, 53121 Bonn, Germany, 1996.